Journal of
Marine Science and Engineering

MDPI

Article

Optimization of Blade Position on an Asymmetric Pre-Swirl Stator Used in Container Ships

Woo-Seok Jin [1], Moon-Chan Kim [1,*], Jin-Gu Kang [1], Yong-Jin Shin [2] and Kyuong-Wan Lee [3]

1 Department of Naval Architecture and Ocean Engineering, Pusan National University, Busan 46241, Republic of Korea
2 Samsung Heavy Industries Co., Ltd., Daejeon 34051, Republic of Korea
3 Technology Part Blue Marine, Busan 46726, Republic of Korea
* Correspondence: kmcprop@pusan.ac.kr; Tel.: +82-51-510-2401

Abstract: Owing to environmental regulations, ships are equipped with a pre-swirl stator (PSS), which is one of the most effective energy-saving devices (ESDs) that is widely applied to various kinds of ships. It improves energy efficiency by recovering the rotational kinetic energy of the propeller with the aid of a PSS placed in front of the propeller. In this study, an asymmetric PSS system is applied to the 2500 TEU eco-friendly liquefied natural gas (LNG) fuel feeder container ship, aimed at optimizing the position of stator blades, using a potential-based program. Additionally, a parametric study was conducted for evaluating the optimum pitch angle and blade spacing. STAR-CCM+ was used for validating the efficiency of the final design. The Samsung towing tank and large cavitation tunnel were also utilized to verify the improvement in the performance of the proposed PSS. Although the efficiency gain is not largely affected by blade position optimization, the cavitation and pressure fluctuation issues are addressed by improving the in-flow to the propeller. Therefore, blade spacing optimization of the stator is important for container ships whose cavitation performance is very significant, especially the relatively high-speed commercial vessels.

Keywords: blade position optimization; pre-swirl stator; energy-saving device; container ships; energy efficiency design index (EEDI)

check for updates

Citation: Jin, W.-S.; Kim, M.-C.; Kang, J.-G.; Shin, Y.-J.; Lee, K.-W. Optimization of Blade Position on an Asymmetric Pre-Swirl Stator Used in Container Ships. *J. Mar. Sci. Eng.* **2023**, *11*, 50. https://doi.org/10.3390/jmse11010050

Academic Editors: Kostas Belibassakis and George Papadakis

Received: 30 November 2022
Revised: 23 December 2022
Accepted: 25 December 2022
Published: 29 December 2022

1. Introduction

Because of their exceedingly high contribution to global warming, greenhouse gas emissions must be curbed by a global collaborative effort from countries and companies to achieve carbon neutrality. For instance, since 2013, the International Maritime Organization (IMO) has been evaluating the Energy Efficiency Design Index (EEDI), which is a measure of the CO_2 emissions from the new ships [1–3]. Additionally, new indices, such as the Energy Efficiency eXisting ship Index (EEXI) and the Carbon Intensity Indicator (CII), which estimate greenhouse gas emissions from the currently operating ships, will be enforced from 2023 [4–6].

Recently, the majority of the container shipping companies have implemented various types of ship fuel efficiency management programs owing to high fuel costs and environmental pollution regulations for container shipments [7]. Particularly, EEDI phase 3, scheduled to be effect in 2025, was applied first to container ships from April 2022. Container ships with more than 20,000 TEU need to be improved by more than 50% compared to the baseline (2013). The fuel efficiency of container ships needs to be urgently improved owing to the aforementioned concerns. However, it is difficult to design an exclusively fuel efficient propeller system because of the cavitation risk in container ships, considering their high speed relative to other merchant ships. Cavitation causes many problems such as ship vibration and erosion. [8,9]. Therefore, propulsion efficiency and cavitation must be simultaneously considered while designing the propulsion system of container ships.

Various methods such as the use of eco-friendly fuels, including liquefied natural gas (LNG) or electricity, improvement of hull shape, and introduction of Energy Saving Devices (ESDs) are being implemented to reduce greenhouse gas emissions from ships. Implementation of ESDs is advantageous from an economic point of view and their viability to the existing vessel, as no major modifications to the design are required. The different types of ESDs used in ships are shown in Figure 1 [10].

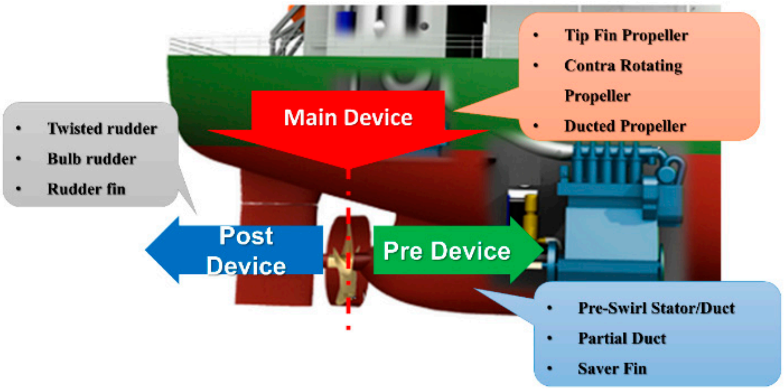

Figure 1. Different types of ESDs used in ships [10].

The pre-swirl stator (PSS) is one of the most effective ESDs that has been widely applied to various kinds of ships. The PSS improves energy efficiency by recovering the rotational kinetic energy of the propeller with the aid of a PSS placed in front of the propeller [11–13]. In general, the PSS has been designed in terms of propulsion efficiency; in addition, recently structural analysis considering the hydrodynamic loads of the PSS blade calculated through CFD has been performed because the reliability becomes important because of frequent applications [14–16]. The rotation of the propeller and upward flow are responsible for the differential flow of fluids on the port and starboard sides; therefore, a different number of blades are introduced on these two sides, leading to an asymmetric PSS structure [17,18]. Recently, several studies, including parametric studies, have been conducted on this asymmetry of the PSS based on various ship types [19–21]; however, no conclusive study has been conducted to estimate an optimized position of the stator blade. Additionally, the asymmetric stator has been studied by varying the number of blades on the port and starboard sides [18,22]. A typical symmetric six-blade stator design consists of three and one blade on the port and starboard sides, respectively, as depicted in Figure 2 [11]. Figure 3 [23] presents a full-scale Mewis duct. We propose that the blade positioning in such a pre-swirl duct can be optimized based on the type of ship and its propeller.

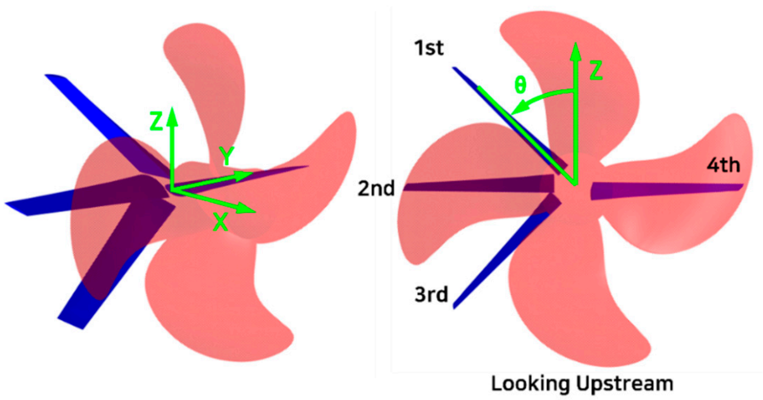

Figure 2. Typical arrangement and coordinate system of the stator blades of an asymmetric PSS.

Figure 3. Photograph of an installed full-scale Mewis Duct [23].

In this study, the optimum pitch angle for the stator was initially designed using the previous asymmetric blade position through a potential analysis program. The equivalent angle of attack (EAOA) [21] is used for the design of the optimum pitch angle in order to have an appropriate load at each blade in order to obtain maximum efficiency gain. After optimizing the blade position, the optimum pitch angle was redesigned for the optimum blade position; this was also validated through the commercial computational fluid dynamics (CFD) analysis tool, named Star-CCM+, followed by the validation of its final design. The design process of the stator is illustrated in Figure 4.

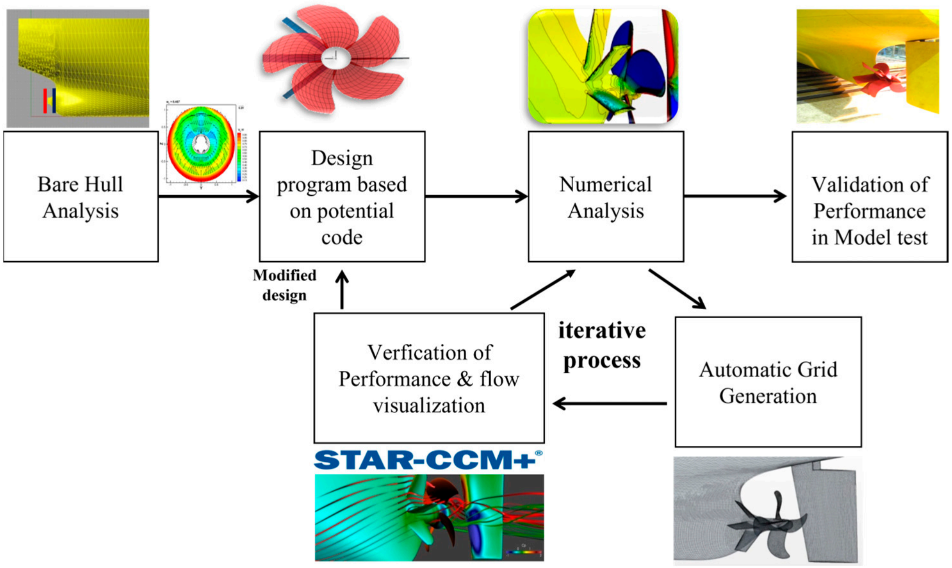

Figure 4. Design process of the PSS.

The propulsion performance of the designed PSS was verified by conducting model and cavitation tests at the towing tank and large cavitation tunnel of the Samsung Heavy Industries (SHI), respectively.

2. Materials and Methods

2.1. Target Ship and Propeller

The target ship is a DS2500TEU LNG fuel feeder container ship provided by Daesun Shipbuilding (Busan, Republic of Korea), and the hull and propeller were designed by the Pusan National University. The model scale and design speed are 27.2 and 19.0 knots, respectively. Table 1 lists the principal parameters of the target and model ship. Figure 5 presents the three-dimensional shape of this ship.

Table 1. Principal parameters of the target ship and its propeller (DS2500TEU LNG fuel feeder Container ship).

	Full Scale	Model Scale
Scale ratio	27.2	
Length PP [m]	185.00	6.801
Length WL [m]	186.30	6.849
Breadth [m]	32.26	1.186
Design Draught [m]	10.00	0.368
W.S.A [m^2]	7351.05	9.936
Design Speed [knots]	19.0	
Propeller Diameter [m]	6.80	0.25
Number of Blades	4	
Mean Pitch Ratio	0.874	
Expanded Area Ratio	0.606	

Figure 5. Three-dimensional shape of the DS2500TEU LNG fuel feeder container ship.

2.2. Numerical Analysis and Validation of the Proposed Design

Various design variables of the PSS, such as the cord length, section shape, blade tip shape, pitch angle for each blade, and diameter of the stator, significantly affect the propulsion efficiency of the ship. Parametric studies focused on the diameter, the number of blades, the axial distance between the stator and propeller, diameter, tip shape, and chord length have been conducted [12,21,24]. In this study, the topic of optimization of the blade position was mainly addressed. Because of the temporal and design-inefficiencies of the CFDs for parametric studies, the potential-based program of the previously developed PASTA code was used in this study [12,13]. The optimum pitch angle estimated by the PASTA code agrees with the experimental results [25]. The PSS was first designed based on the existing typical blade position (see Figure 6), followed by the optimization of the stator blade position. Subsequently, the pitch angle was redesigned based on the optimized position. The validation of the performance with the redesigned stator was conducted through CFD analysis (Star-CCM+) and model tests.

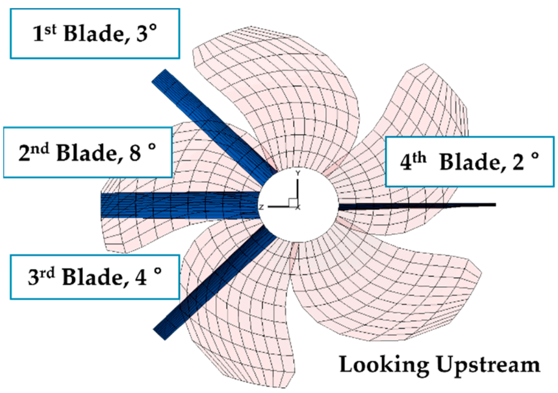

Figure 6. Optimal pitch angle of each blade in the initial PSS.

The non-uniform wake data were used for analysis using the PASTA program. The concept of EAOA was used to calculate and visualize the load on each blade to facilitate the design of the pitch angle [17,24]. Because the blades are placed in the non-uniform flow field of the stern, the performance of the PSS is negatively affected owing to the difference in the hydrodynamic pitch angle of each blade and the magnitude of the load, even if all the blades have the same pitch angle. In previous studies [21,24], the efficiency was found to be the highest when the maximum EAOA of the PSS was approximately 12° for the container ship. Therefore, in this study, a maximum EAOA of 12° was also applied.

The 1800 TEU container ship similar to the present container ship was selected for validation by comparing the model test results to confirm the present analysis system. The present LNG fuel container feeder ship was also validated by comparing the model tests. The model test of the 1800 TEU container ship was conducted in the Samsung Ship Model Basin (SSMB); the principal parameters of the mother ship are listed in Table 2. The analysis conditions are presented in Table 3, and the boundary conditions and grid system are shown in Figure 7. The commercial code of Star-CCM+ was used for the present computations (resistance, POW, and self-propulsion), wherein the Reynolds stress model was applied for the turbulence model. In the present grid system, three cases for the y+ of 50, 100, and 200 were compared, and the case of 200 was chosen because of good correlation with the experimental results. Table 4 presents a comparison of the self-propulsion results obtained between the computation and model tests without using a stator. There exists some discrepancy in the thrust deduction factor; however, the excellent agreement can be observed in η_D, which implies that the present computation tool can be applied to the present LNG container feeder ship, especially for predicting its efficiency.

Table 2. Principal parameters of the mother ship and propeller (1800 TEU Container Ship).

	Full Scale	Model Scale
Scale ratio	26.4	
Length PP [m]	163.00	6.17
Length WL [m]	160.59	6.08
Breadth [m]	27.50	1.04
Design Draught [m]	8.75	0.33
W.S.A [m^2]	5591.00	8.02
Design Speed [knots]	19.0	
Propeller Diameter [m]	6.60	0.250
Number of Blades	5	
Mean Pitch Ratio	0.952	
Expanded Area Ratio	0.625	

Table 3. Computational conditions for the analysis of the 1800 TEU container ship.

Analysis Conditions	
Program	Star-CCM+ (Ver 11.02)
Governing Equation	Incompressible RANS Equation
Discretization	Cell Centered FVM
Turbulence model	Reynolds Stress Model
Wall function	Non-Equilibrium
Rotation method	Sliding Moving Mesh
Velocity-Pressure Coupling	SIMPLE Algorithm
Number of Mesh	8,000,000
y+	200

Table 4. Comparison of self-propulsion results between experimental fluid dynamics (EFD) and computational fluid dynamics (CFD) of the 1800 TEU container ship.

	w_{TS}	t	η_O	η_R	η_H	η_D
EFD (SSMB) [1]	0.266	0.186	0.706	1.035	1.111	0.810
CFD (PNU) [2]	0.268	0.201	0.701	1.055	1.093	0.809

[1] Experimental fluid dynamics (Samsung Ship Model Basin); [2] computational fluid dynamics (Pusan National University).

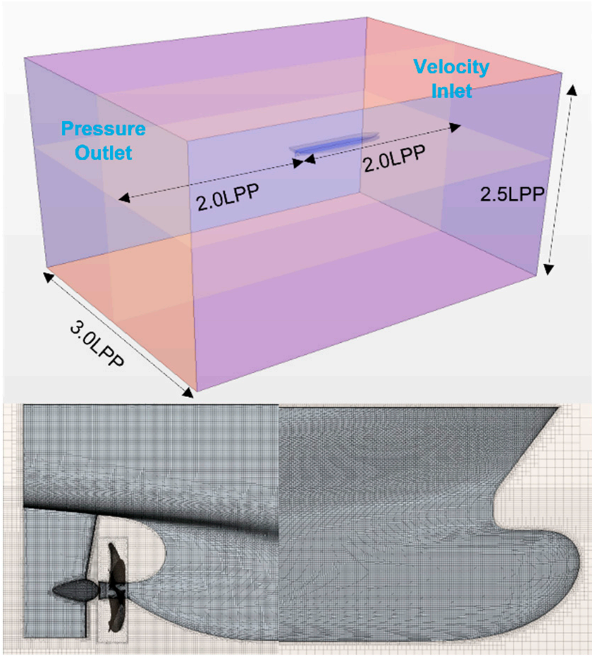

Figure 7. Boundary condition and grid system of the 1800 TEU Container Ship.

2.3. Optimization of the PSS Design

2.3.1. Initial Design of PSS

The PSS is a representative counter-swirl pre-device attached to the front of the propeller. The design parameters of the initial PSS include the dimensions of the blade section, diameter, number of blades, distance to the propeller, and the attachment pitch angle of each blade as mentioned before. The initial PSS was designed using the results verified through previous studies [12,17,21,24,26].

The chord length, which is the main variable of the blade section of the PSS, was determined by applying the relationship between the nominal wake ratio and chord length derived through the PSS optimization study based on the ship type [24]. A previous study [26] designed a compact PSS for the KRISO container ship (KCS), a container ship similar to the target ship of this study, and increased its propulsion efficiency. Therefore, the chord, camber, and thickness of the PSS were designed by scaling the verified specifications of Shin's PSS [24] according to the difference in its mean wake.

The diameter (same as that of the propeller) and the distance (0.5 R of the propeller) between the propeller and the PSS have been studied by [22]. For optimizing the attachment position of each blade, angles such that the θ of Figure 2 are 45°, 90°, 135°, and 270° were applied for the initial design [17]. The initial PSS specifications were determined based on the non-dimensionalized specifications of the PSS for KCS, which are similar to the target ship, and are summarized in Table 5. The optimally determined pitch angle for the initial position of the PSS is shown in Figure 6, where the EAOA was calculated using the potential code (PASTA) as mentioned before. As shown in Table 6, the propulsion efficiency according to the application of the initial PSS is increased by approximately 2.39 % of the delivered horsepower by the present CFD computation.

Table 5. Non-dimensionalized specifications of the initially designed stator.

	0.2	**0.25**	**0.3**	**0.4**	**0.5**	**0.6**	**0.7**	**0.8**	**0.9**	**0.95**	**1.0**
Chord/Diameter	0.177	0.174	0.171	0.165	0.159	0.153	0.147	0.142	0.136	0.133	0.130
Camber/Chord	0.085	0.082	0.078	0.071	0.063	0.054	0.045	0.035	0.024	0.019	0.013
Thickness/Diameter	0.037	0.035	0.033	0.030	0.026	0.023	0.019	0.016	0.012	0.011	0.009

Table 6. Comparison of performances with and without the initially designed PSS by CFD.

	n_m (rps)	Q_m (Nm)	$2\pi n_m Q_m$ (W)	Diff (%)
Bare	8.28	1.58273	82.34	-
w/PSS	7.93	1.61248	80.37	−2.39

2.3.2. Final Design of PSS

Blade Position

The blade positions of the asymmetric PSS are generally decided at 45°, 90°, 135° on the port side, and 270° on the starboard side, as shown in Figure 6. Takekuma et al. [11] proposed a six-blade symmetric PSS, which has the same angle position at both sides (port: 45°, 90°, and 135°; starboard side: 225°, 270°, and 315°). The two blades (top and bottom) at the starboard side were removed because of the cancellation of the tangential velocity by upward flow at a stern region of a hull for the asymmetric stator. However, this position of all blades has not been precisely decided in consideration of recovering the tangential velocity of the hull and propeller, as shown in Figure 8. The optimal position of the blade was determined by varying the position angle using the developed potential code (PASTA).

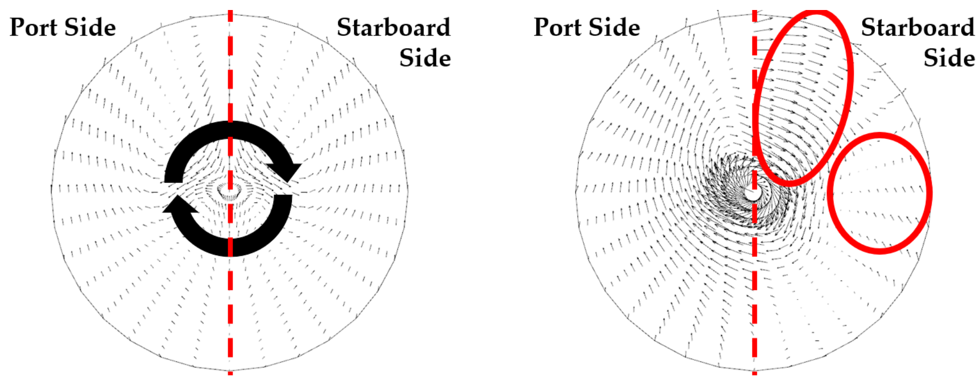

(**a**) (**b**)

Figure 8. Tangential component of wake distribution (**a**) without the propeller; (**b**) with the propeller.

The process of optimizing the position of each blade is shown in Figure 9. First, the pitch angle and the other parameters were designed through the previous studies [12,17,21,24,26] with the previous blade position (45°, 90°, 135°and 270°). The range and interval of each blade were set and the computation with the combination of each case was conducted to have the optimum EAOA, which is closely related with the optimum efficiency [21,24]. Finally, the pitch angle was redesigned with the selected optimum blade position.

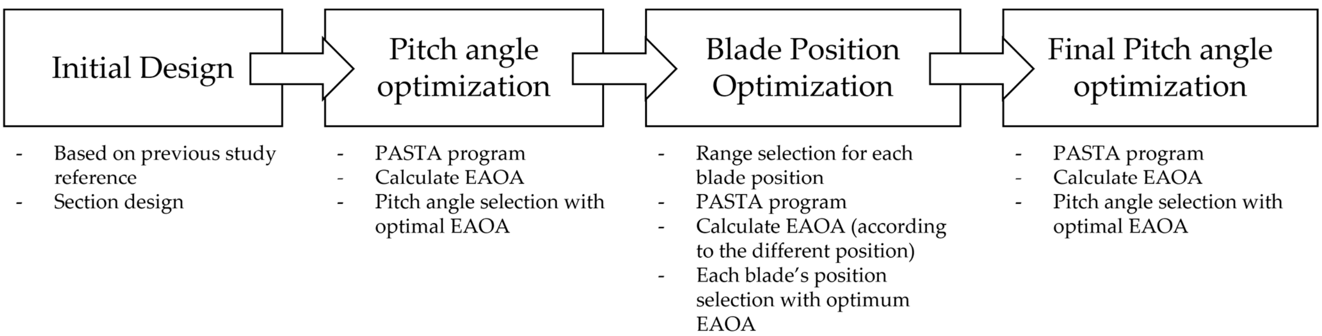

Figure 9. Blade Position Optimization Procedure.

As shown in Figure 10, the ranges of the blade angles at the port side were set to 20–110° for b1, 40–130° for b2, and 60–150° for b3, and the range at the starboard side was set in the range from 220 to 320° for b4 for optimizing the position of the blades. The interval of the angle range was set to 5°, retaining the sequence of the blades. Approximately 28,000 combinations of analysis cases for optimization were performed by the PASTA potential code. As shown in Table 7, the maximum loading (the average of the EAOA) for each blade can be obtained at 40° for b1, 90° for b2, 150°for b3, and 290° for b4.

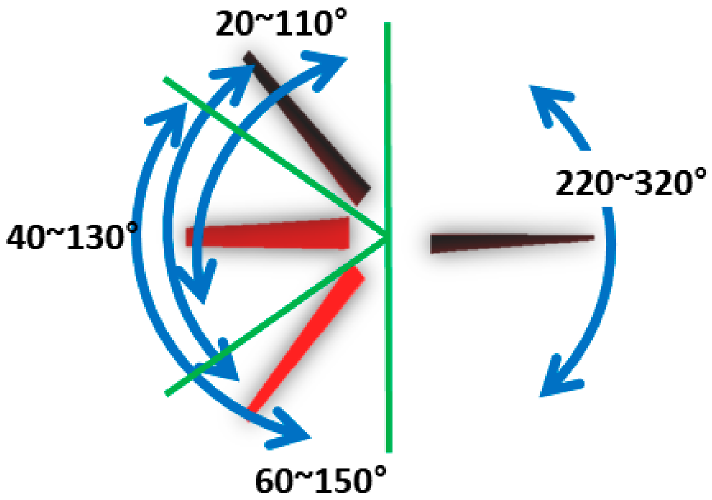

Figure 10. Range of angles for the optimization of the blade position (looking upstream).

Table 7. Equivalent angle of attack of each blade calculated by the potential program for some typical cases (**bold face** is the most optimum case).

Case (Degree)	KT	Equivalent Angle of Attack (Degree)				
		1st Blade	2nd Blade	3rd Blade	4th Blade	Average
40/90/150/290	**0.224**	**−11.29**	**−11.74**	**−12.18**	**−14.30**	**−12.38**
35/100/150/290	0.224	−11.59	−11.82	−11.71	−14.26	−12.34
35/85/150/265	0.223	−11.25	−11.91	−12.27	−13.49	−12.23
35/85/150/285	0.221	−10.92	−11.71	−12.17	−14.09	−12.22
35/80/150/285	0.221	−10.68	−11.74	−12.34	−14.10	−12.21
			⋮			
100/120/140/220	0.205	−7.00	−8.77	−8.73	−12.37	−9.22
105/125/145/220	0.206	−6.99	−8.99	−8.64	−12.24	−9.22
110/130/150/220	0.206	−7.05	−9.15	−8.51	−12.09	−9.20
25/45/65/320	0.205	−7.38	−8.11	−8.27	−13.00	−9.19
20/40/60/320	0.207	−7.05	−8.25	−8.14	−12.76	−9.05

To investigate the physics of the blade position optimization, the tangential velocity components at the stator plane and the plane behind 0.25 D (diameter) from the propeller were analyzed through CFD self-propulsion analysis without using a stator, as shown in Figure 11. A large tangential velocity component (upward flow) is generated at the 70° and 295° positions by the hull at the stator plane. Further, at the plane behind 0.25 D from the propeller, the upward flow by the hull is in the same direction as the propeller rotation on the port side. Accordingly, Thus, the tangential velocity increases at 40–150° starboard, cancels out at 200–270° port, but is still large at the 350° position. Therefore, it is necessary to increase the propulsion efficiency of the PSS to recover the largely remaining tangential velocity in these regions. The positions of b1, b2, b3, and b4 are optimally decided to be 40°, 90°, 150°, and 290°, respectively, through the potential program. The overall tangential velocity component of the PSS case is less compared to the without stator case, as shown in

Figure 12, where the red line indicates the position of each blade. Because of optimizing the location for each blade, the efficiency increased by approximately 0.6% compared to the initial PSS.

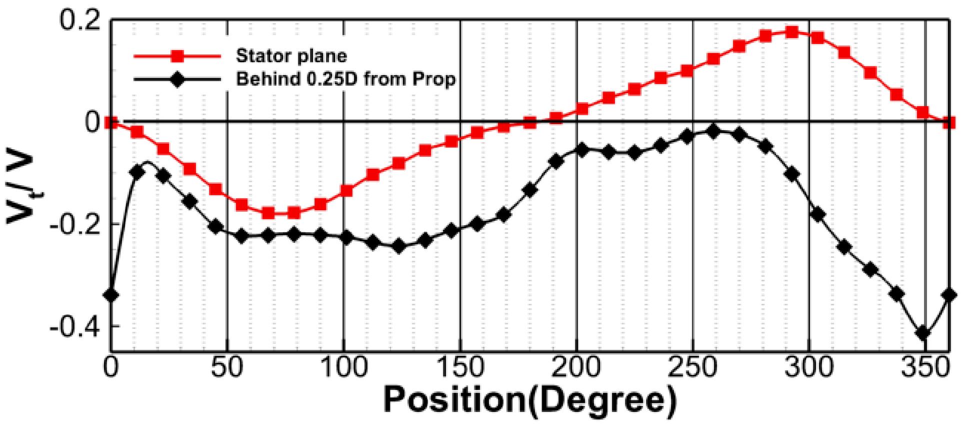

Figure 11. Averaged circumferential tangential velocity at stator plane and the plane behind 0.25 D from propeller (with propeller, without stator).

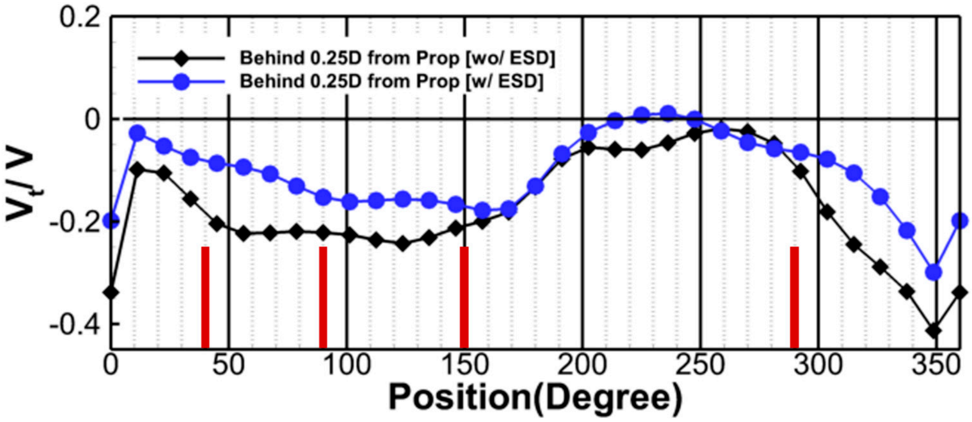

Figure 12. Averaged circumferential tangential velocity component at plane behind 0.25 D from propeller (without propeller).

For example, in case of the fourth stator blade, the remaining tangential velocity exists around the position of 350°, which is different from the optimized position (290°) of the fourth blade, as shown in Figure 12. As the stator position is half of the propeller radius ahead of the propeller position, the flow from the stator turns along the stator surface roughly between the pressure side and the mean camber line to the propeller, as shown in Figure 13. The turning angle of the flow is approximately 60° from the fourth blade of the stator to the propeller; therefore, the optimized stator angular position was determined to be 290°. The configuration of the optimized stator is shown with the previous stator in Figure 14.

Tip Rounding

There are various problems regarding the tip vortex and tip vortex cavity of the stator blades, such as vibration, noise, and erosion that sometimes cause serious damage to the propeller and rudder. To solve this problem, the occurrence of the tip vortex can be reduced by applying a rounding blade tip shape, wherein the cross-sectional chord length of the blade tip approaches 0. We applied the design method incorporating the equation of the ellipse proposed in a previous study [26], and the starting part of the round shape was designed to be 0.9 R. The final designed three-dimensional modeling shape is shown in

Figure 15. Although the counter-swirl at the tip is weakened because of tip rounding, the efficiency is increased by 0.22 %. This is attributed to the reduction in the tip's drag. The tip rounding application seems effective as it enhances the efficiency for this container ship, which is relatively faster than other merchant ships.

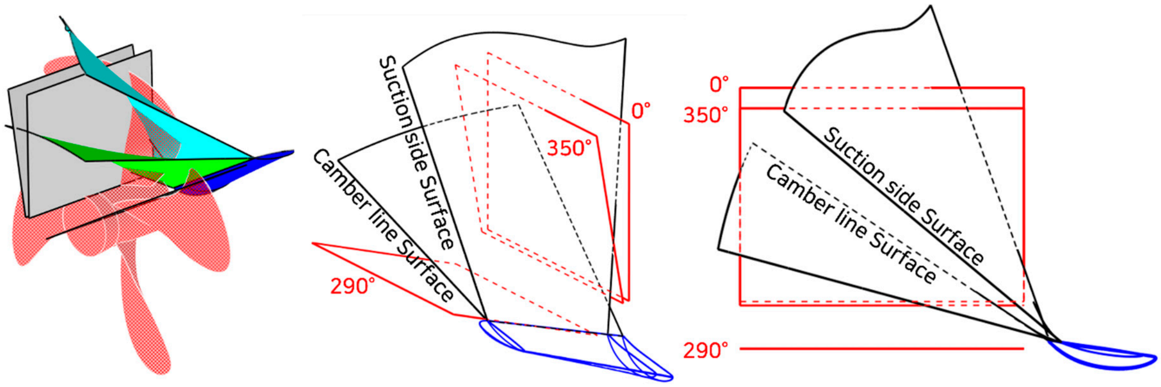

Figure 13. Illustration of the difference in the flow angle between the stator and propeller position (fourth blade stator).

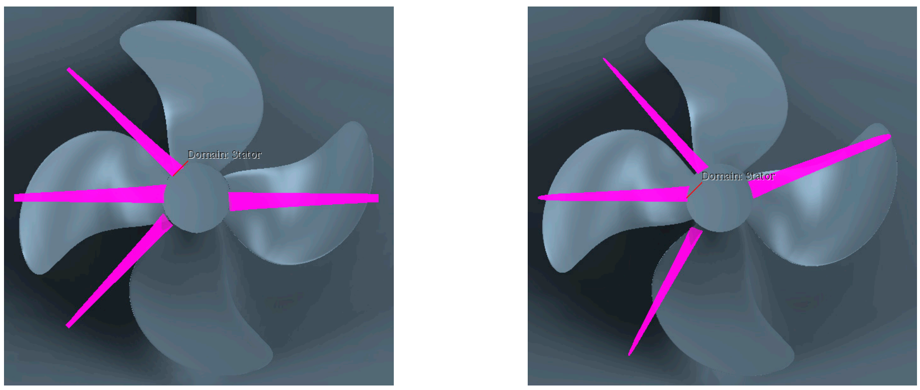

(**a**) (**b**)

Figure 14. Comparison of profile (looking upstream) (**a**) Previous position (45°, 90°, 135°, 270°); (**b**) Optimized position (40°, 90°, 150°, 290°).

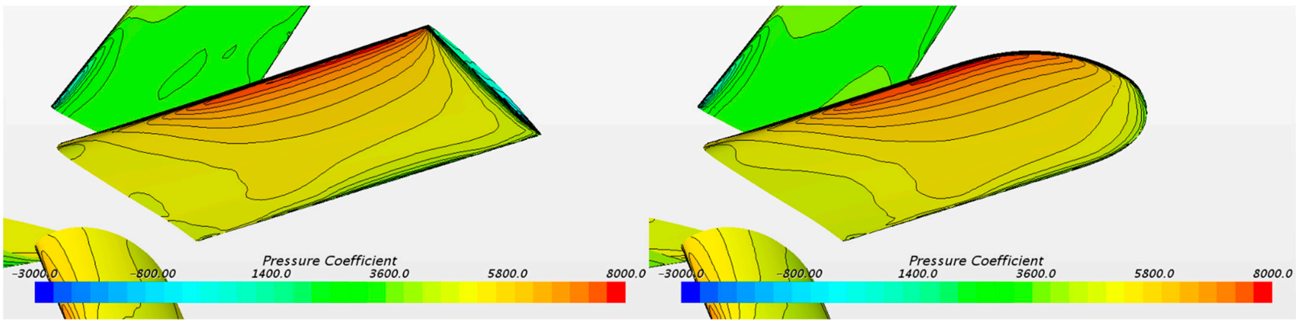

Figure 15. Comparison of the tip configuration and pressure distribution with and without the tip rounding treatment.

3. Results and Discussion

3.1. Comparison of CFD Result

Various scenarios, such as tip rounding, optimization of the blade position, and a combination of these, were computed by the CFD to compare their performances, and are shown in Table 8. Our results show that on applying tip rounding and position optimization, the efficiency improves by 0.13% and 0.59% compared to the reference, respectively. Finally, with the optimized stator (Case 3), a gain of 3.23% was obtained compared to the bare hull case (without stator). The bulb-type rudder was applied to the final application instead of the full-spade plain rudder (Case 4), as shown in Figure 16. A 0.33% gain was obtained with the bulb-type rudder (Case 4) in comparison with Case 3, and finally, a 3.56% gain was achieved compared to the bare hull case (without stator and with full-spade plain rudder) by the CFD computation. The bulb-type rudder was adopted for the actual project; note that a detailed description of the bulb design is omitted in the present study (see [27]).

Table 8. Comparison of propulsive performances according to the case study by CFD.

Case		Design Parameter		Performance			
		Blade Position	**Tip Rounding**	n_m (rps)	Q_m (Nm)	$2\pi n_m Q_m$ (W)	**Diff (%)**
Bare Hull		N/A	N/A	8.28	1.58273	82.34	-
Pre-Swirl Stator	Reference	45/95/135/270	N/A	7.93	1.61248	80.37	−2.39
	Case 1	40/90/150/290	N/A	7.97	1.59588	79.89	−2.98
	Case 2	45/95/135/270	0.9R	7.81	1.63599	80.27	−2.52
	Case 3	40/90/150/290	0.9R	7.95	1.59563	79.68	−3.23
Combined ESD	Case 4	40/90/150/290	0.9R	7.93	1.59426	79.41	−3.56

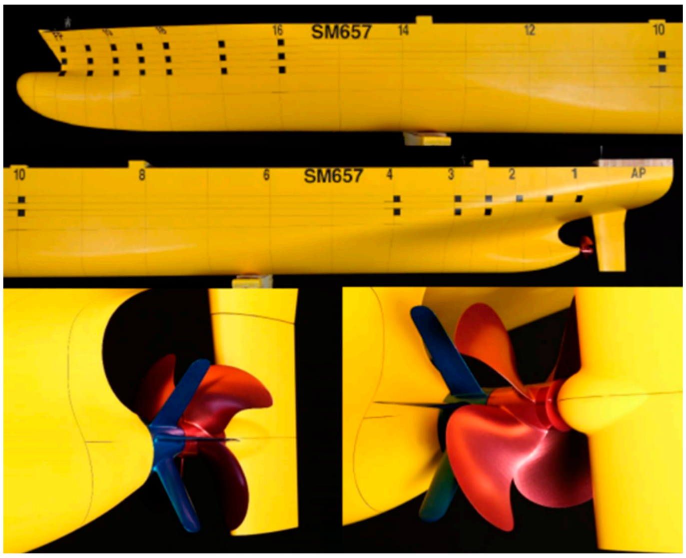

Figure 16. Model ship equipped with a PSS, propeller, and bulb-type rudder.

3.2. *Performance Validation through Model Test*

3.2.1. Test Condition

The model test was carried out for the final optimized Case 4 in the towing tank of SHI (L × B × D: 400.0 × 14.0 × 7.0 m). The scale ratio of the model ship is 27.2, which is the same as the scale ratio used in the CFD analysis, and the principal dimensions of the target ship are shown in Table 1. The model was mounted onto the carriage free to heave, roll, and pitch, and was fixed in a surge, sway, and yaw motion by using two trim guides. The model test cases were conducted with and without an ESD [27].

3.2.2. Analysis of the Model Test Results

The model test results at the SSMB are compared with the CFD results. The International Towing Tank Conference (ITTC) 1957 two-dimensional method [28] was applied to the evaluation of the full-scale resistance, which was recently used for the ESD case because the form factor is delicately dependent on the additional device. The ITTC 1999 method [29] was also applied to the evaluation of the full-scale self-propulsion results, which is particularly used for the pre-swirl stator. There is a good correlation between the CFD and the experimental results of with and without the ESD. The gain of the delivered power with the ESD is 3.96 % compared to the bare hull case by the model test results, which is also similar to the gain of 3.56 % by the CFD. Although there exists a slight difference in the propulsive factors between the CFD and the experimental results, the quasi-propulsion efficiency is comparable between the two, as shown in Table 9.

Table 9. Comparison of the self-propulsion results between the SSMB model test result and CFD computation.

Case		P_D (kW)	w_{TM}	w_{TS}	t	η_H	η_R	η_O	η_D
Bare	CFD	9415	0.292	0.288	0.243	1.062	1.054	0.684	0.766
	EFD	10,141	0.273	0.246	0.180	1.087	1.015	0.689	0.761
w/ESD	CFD	9094	0.375	0.370	0.268	1.163	1.065	0.648	0.803
	EFD	9739	0.342	0.315	0.192	1.179	1.020	0.664	0.799

3.3. Comparison of Cavitation Performance by Model Test

3.3.1. Test Condition

To investigate the effect of the cavitation performance, including the pressure fluctuation with the optimized stator, a cavitation test was conducted in Samsung CAvitation Tunnel (SCAT). The test section size of SCAT is 12.0 × 3.0 × 1.4 m, and the maximum flow speed is 12.0 m/s. The parameters of the test condition were determined using the torque identity method from the previous results of the powering performance tests in the towing tank. For the calculation of the cavitation number, the hydrostatic pressure at the radius of 0.7 R in the 12 o'clock blade position was considered, including a stern wave of 1.3 m in height. The pressure fluctuations were also simultaneously measured. The seven pressure transducers were flush-mounted inside the ship model above the propeller, as shown in Figure 17. The test conditions are summarized in Table 10.

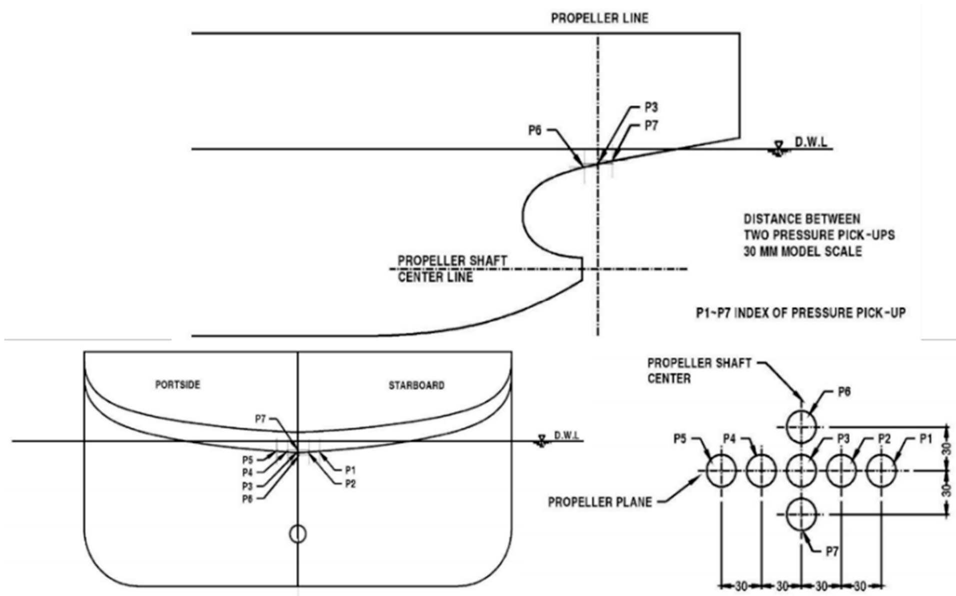

Figure 17. Position of the pressure transducers on the hull surface.

Table 10. Test conditions for the cavitation test.

Item	Bare	w/ESD
Draught at Stern [m]	10.0	
Stern Wave Height [m]	1.3	
NCR Power [kW]	11,798	
Sea Margin [%]	15	
Number of Revolutions [rpm]	103.70	101.8
Ship Speed [knots]	19.01	19.21
Advance Coefficient, J_A	0.6276	0.5912
Thrust Coefficient, K_T	0.1731	0.1903
Cavitation Number at 0.7R, σ_n	2.1611	2.2746

3.3.2. Analysis of Model Test Results

The photographs of the cavity patterns based on the angular positions are shown in Figures 18 and 19. It is clearly seen that the amount of cavity around the top position, especially the tip region, is reduced by applying the present PSS. These cavities obviously affect the pressure fluctuation on the hull surface, as shown in Figure 20. As the cavity is stable, the pressure fluctuation value of the first blade rate frequency is much higher than the others (second to fifth). The maximum value is found at P2, which slightly shifts in the starboard direction (Figure 17). This appears to be reasonable because the cavity collapses at the starboard side in spite of the top position being nearest to the hull surface. The maximum values of the two cases, that is, without the stator and with the stator, are 2.74 kPa and 2.31 kPa, respectively. A greater than 10% reduction in pressure fluctuation was achieved using the proposed optimized stator.

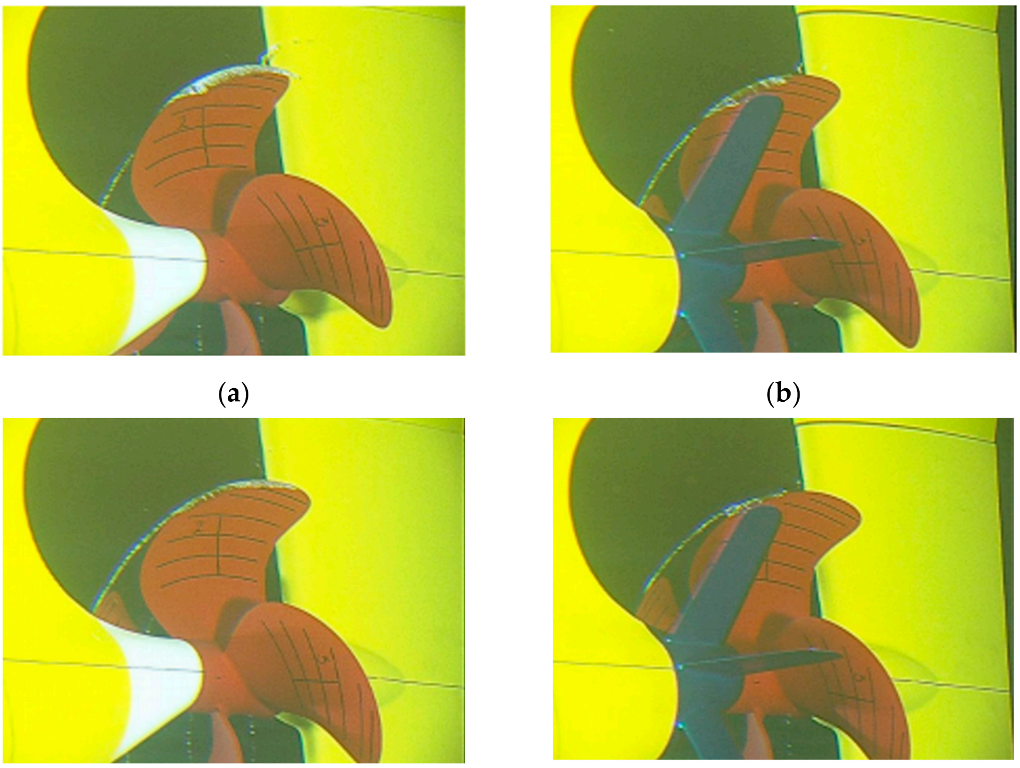

(**a**) (**b**) (**c**) (**d**)

Figure 18. Photos of cavity for Bare and with ESD (**a**,**b**) $\theta = 0°$; (**c**,**d**) $\theta = 10°$.

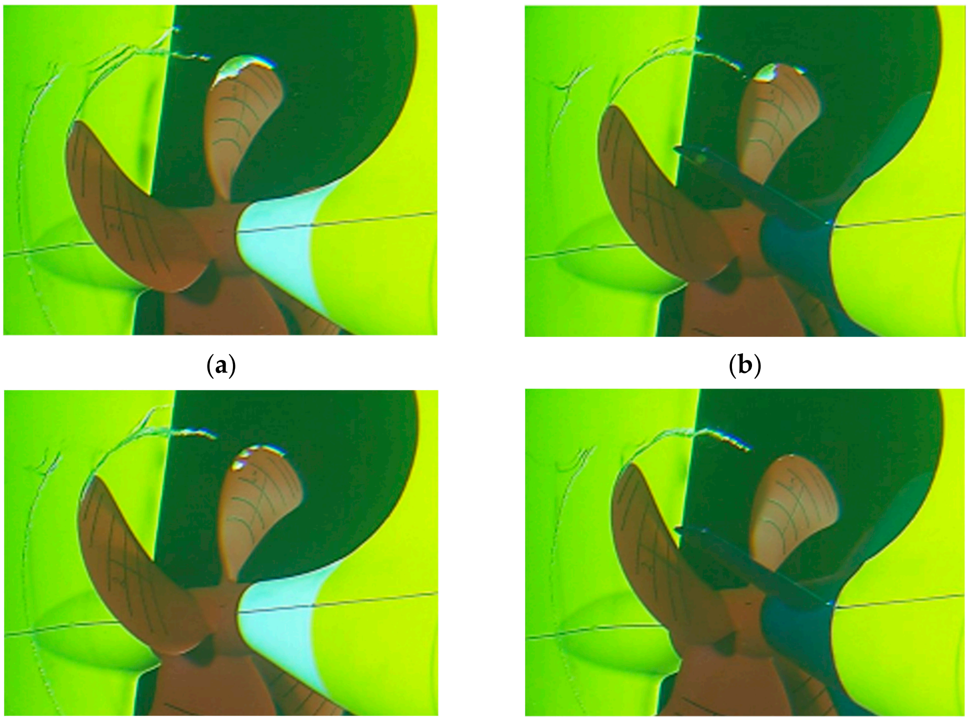

(a) (b)

(c) (d)

Figure 19. Photos of cavity for Bare and with ESD (**a**,**b**) $\theta = 280°$; (**c**,**d**) $\theta = 290°$.

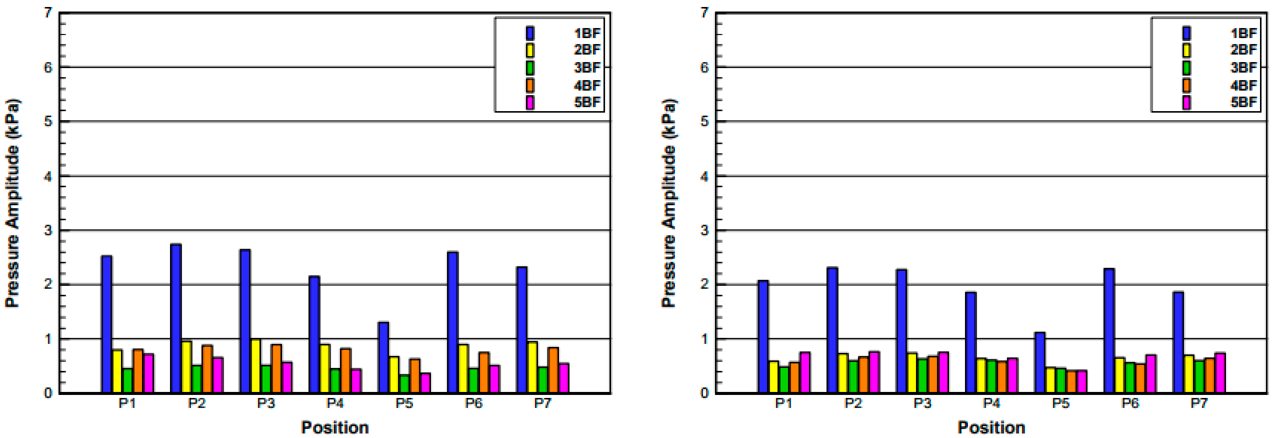

(**a**) (**b**)

Figure 20. Full-scale pressure fluctuations, first to fifth blade frequency at seven designated points (**a**) Bare; (**b**) with ESD.

4. Conclusions

In this study, the optimum position of the stator blade was evaluated. The DS2500TEU LNG fuel feeder container ship was chosen as the target ship. After the reference stator was designed based on previous studies [12,17,21,24,26], blade position optimization was conducted through the potential-based program by the variation of 2800 cases to achieve the highest efficiency. The CFD computations were applied to validate the selected stator with the optimum spacing blade and to investigate the flow phenomena based on different positions. The previous position of the stator blade was three blades on the port (45°, 90°, 135°) and one blade on the starboard (270°) sides. The optimized stator blade position is rather similar to the above-mentioned positions, which are 40°, 90°, and 150° on the port side and 290° on the starboard side. The correlation between the retained tangential velocity and stator blade position was investigated to confirm the optimized position. The optimized stator plays a role in the cancellation of the tangential velocity, although the angular position of the stator is different from the retained tangential velocity behind the propeller plane because the fluid flows along the pitch angle line of the stator. Although the real viscous effect is not included in the potential code, the optimization of the blade position improves the efficiency because the potential behavior (tangential velocity) is dominant in the stator problem if the separation does not occur.

Regarding the efficiency gain, +0.59% was achieved by the blade position optimization compared to the previous position by the CFD computation. With tip rounding, an additional 0.13% efficiency gain is obtained compared with and without tip rounding. Finally, a 3.56% efficiency gain was achieved with the stator and rudder bulb (bulb gain is 0.33%). Although there is little improvement in efficiency by position optimization, the flow becomes more unified upon using the optimized stator, which consequently improves the cavity performance. This was also verified through the cavitation test in a large cavitation tunnel (SCAT).

Model tests (POW, resistance, and self-propulsion) were conducted with the optimized stator, including tip rounding and rudder bulb, to validate the effect of the optimized stator. The delivered power improves by 3.96% compared to the reference (without stator and plain full-spade rudder), which is similar to the gain of the CFD computation. A cavitation test including the pressure fluctuation measurement was also executed in the large cavitation tunnel to study the stator effect on the cavitation of the propeller. The amount of cavity decreased at every angular position with the stator whose effect is clearly shown at pressure fluctuation. Using the stator, pressure fluctuation decreases by more than 10%. The present stator blade optimization plays a role in enhancing the cavity by unifying the flow and improving its efficiency. The comparison of the cavity and pressure fluctuation between the model tests and CFD computation is also expected to be conducted in the near future.

Author Contributions: Conceptualization, M.-C.K.; validation, Y.-J.S. and W.-S.J.; investigation, Y.-J.S. and K.-W.L.; resources, M.-C.K.; writing—original draft preparation, W.-S.J. and J.-G.K.; writing—review and editing, W.-S.J. and M.-C.K.; visualization, W.-S.J. and J.-G.K.; supervision, M.-C.K.; project administration, W.-S.J.; funding acquisition, M.-C.K.; All authors have read and agreed to the published version of the manuscript.

Funding: This research was funded by the Korea Institute of Energy Technology Evaluation and Planning (KETEP) and the Ministry of Trade, Industry and Energy (MOTIE) of the Republic of Korea (20224000000090) and was also supported by Basic Science Research Program through the National Research Foundation of Korea (NRF) funded by the Ministry of Science, ICT and Future Planning (NRF-2022R1F1A1070993).

Institutional Review Board Statement: Not applicable.

Informed Consent Statement: Not applicable.

Data Availability Statement: Not applicable.

Conflicts of Interest: The authors declare no conflict of interest.

References

1. Ekanem Attah, E.; Bucknall, R. An analysis of the energy efficiency of LNG ships powering options using the EEDI. *Ocean. Eng.* **2015**, *110*, 62–74. [CrossRef]
2. Ancic, I.; Sestan, A. Influence of the required EEDI reduction factor on the CO2 emission from bulk carrier. *Energy Policy* **2015**, *84*, 107–116. [CrossRef]
3. Vladimir, N.; Ancic, I.; Sestan, A. Effect of ship size on EEDI requirements for large container ships. *J. Mar. Sci. Technol.* **2018**, *23*, 42–51. [CrossRef]
4. Ivanova, G. Analysis of the specifics in calculating the index of existing marine energy efficiency EEXI in force since 2023. In Proceedings of the 13th Electrical Engineering Faculty Conference, Resort „St.St. Constantine and Elena, Varna, Bulgaria, 8–11 September 2021; pp. 1–4.

5. Perera, L.P.; Ventikos, N.P.; Rolfsen, S.; Anders, O. Advanced data analytics towards energy efficient and emission reduction retrofit technology integration in shipping. In Proceedings of the 31st International Ocean and Polar Engineering Conference, Rhodes, Greece, 20 June 2021.
6. Wang, S.; Psaraftis, H.N.; Qi, J. Paradox of international maritime organization's carbon intensity indicator. *Commun. Transp. Res.* **2021**, *1*, 100005. [CrossRef]
7. Meng, Q.; Du, Y.; Wang, Y. Shipping log data based container ship fuel efficiency modeling. *Transp. Res. Part B* **2016**, *83*, 207–229. [CrossRef]
8. Peters, A.; Lantermann, U.; Moctar, O. Numerical prediction of cavitation erosion on a ship propeller in model- and full-scale. *Wear* **2018**, *408*, 1–12. [CrossRef]
9. Berteta, D.; Brizzolara, S.; Gaggero, S.; Viviani, M.; Savio, L. CPP propeller cavitation and noise optimization at different pitches with panel code and validation by cavitation tunnel measurements. *Ocean. Eng.* **2012**, *53*, 177–195. [CrossRef]
10. Kang, J.G.; Kim, M.C.; Shin, Y.J. Study on compact pre-swirl duct for slender aft-body crude oil carrier. *J. Mar. Sci. Eng.* **2022**, *10*, 396. [CrossRef]
11. Takekuma, K.; Tsuda, S.; Kawamura, A.; Kawaguchi, N. Development of reaction fin as a device for improvement of propulsive performance of high block coefficient ships. *J. SNAJ* **1981**, *150*, 30–44. [CrossRef] [PubMed]
12. Lee, J.T.; Kim, M.C.; Suh, J.C.; Kim, S.H.; Choi, J.K. Development of a preswirl stator-propeller system for improvement of propulsion efficiency: A symmetric stator propulsion system. *J. Soc. Nav. Archit. Korea* **1992**, *29*, 132–145.
13. Kim, M.C.; Lee, J.T.; Suh, J.C.; Kim, H.C. A study on the asymmetric pre-swirl stator system. *J. Soc. Nav. Archit. Korea* **1993**, *30*, 30–44.
14. Bakica, A.; Vladimir, N.; Jasak, H.; Kim, E.S. Numerical simulations of hydrodynamic loads and structural responses of a Pre-Swirl Stator. *Int. J. Nav. Archit. Ocean. Eng.* **2021**, *13*, 804–816. [CrossRef]
15. Bakica, A.; Vladimir, N.; Malenica, S.; Im, H.I. Numerical procedure for pre-swirl stator structural integrity evaluation. *Ocean. Eng.* **2022**, *258*, 12. [CrossRef]
16. Bakica, A.; Malenica, S.; Vladimir, N.; Senjanovic, I. Hydroelastic analysis of pre-swirl stator. *Mar. Struct.* **2022**, *85*, 13. [CrossRef]
17. Kim, M.C.; Chun, H.H.; Kang, Y.D. Design and Experimental Study on a New Concept of Preswirl Stator as an Efficient Energy-Saving Device for Slow Speed Full Body Ship. In Proceedings of the 2004 SNAME Annual Meeting, Washington, DC, USA, 30 September 2004.
18. Kang, Y.D.; Kim, M.C.; Chun, H.H. A study on the design of a biased asymmetric pre-swirl stator propulsion system. *J. Soc. Nav. Archit. Korea* **2004**, *41*, 13–21.
19. Lee, C.M.; Shin, Y.J.; Kim, M.C.; Choi, J.E.; Chun, H.H. Design of asymmetric pre-swirl stator for LNG carrier according to variation of stator shapes. *J. Soc. Nav. Archit. Korea* **2016**, *53*, 37–44. [CrossRef]
20. Lee, K.S.; Kim, M.C.; Shin, Y.J.; Kang, J.G. Design of asymmetric pre-swirl stator for KVLCC2 considering angle of attack in non-uniform flow fields of the stern. *J. Soc. Nav. Archit. Korea* **2019**, *56*, 352–360. [CrossRef]
21. Shin, Y.J.; Kim, M.C.; Kang, J.G.; Kim, H.U.; Shin, I.R. Validation of optimally designed stator-propeller system by EFD and CFD. *Brodogr. Teor. I Praksa Brodogr. I Pomor. Teh.* **2019**, *70*, 133–151. [CrossRef]
22. Lee, J.T.; Kim, M.C.; Van, S.H.; Kim, K.S.; Kim, H.C. Development of a Preswirl Stator Propulsion System for a 300K VLCC. *J. Soc. Nav. Archit. Korea* **1994**, *31*, 1–13.
23. Becker Mewis Duct. Available online: https://www.becker-marine-systems.com/products/product-detail/becker-mewis-duct.html (accessed on 29 November 2022).
24. Shin, Y.J. A Study on the Analysis of Interactions and Optimal Design of Energy Saving Devices by Ship Types. Ph.D. Thesis, Pusan National University, Busan, Republic of Korea, 2019.
25. Kwon, J.I. A Study on the Biased Asymmetric Pre-swirl Stator for a Container Ship. Master's Thesis, Pusan National University, Busan, Republic of Korea, 2013.
26. Shin, Y.J.; Kim, M.C.; Kang, J.G.; Lee, J.H. Study on Performance of Asymmetric Pre-Swirl Stator according to Variations in Dimensions and Blade Tip Shape. *J. Ocean. Eng. Technol.* **2016**, *30*, 431–439. [CrossRef]
27. Lee, S.G.; Cho, S.J.; Ha, W.H.; Lee, I.W.; Kim, H.T.; Lee, K.W. *Development of Hull Form and Basic Design with Energy Saving Device for LNG Fueled Feeder Container Ship*; TRKO202200005831; Ministry of Trade, Industry and Energy: Sejong City, Republic of Korea, 2021.
28. International Towing Tank Conference. 1978 ITTC Performance Prediction Method. In Proceedings of the 29th ITTC, Online, 13–18 June 2021.
29. International Towing Tank Conference. Scaling method for ship wake fraction with pre-swirl devices. In Proceedings of the 29th ITTC, Online, 13–18 June 2021.